Maximum power point tracking (MPPT) of a scale-up pressure retarded osmosis (PRO) osmotic power plant

Wei He, Yang Wang, and Mohammad Hasan Shaheed[1]

School of Engineering and Materials Science, Queen Mary, University of London, London E1 4NS, UK

Abstract:

This paper presents a Maximum power point tracking (MPPT) of a scale-up pressure retarded osmosis (PRO) based osmotic power generator. Inspired by the well-known MPPT in photovoltaic (PV) array, two algorithms, perturb & observe (P&O) and incremental mass-resistance (IMR) method, are investigated. Using a series of simulations, both the algorithms are demonstrated to be capable of tracking the maximum power point (MPP) and capturing the transitions between varied MPPs due to the fluctuations of operating temperature. However, in both cases the trade-off between the rise time and the oscillation is found requiring further consideration on the selection of the step-size for perturbation pressure or incremental pressure. In order to improve the performance of the MPPT, furthermore, an optimum model-based controller (OMC) is used to estimate the initial optimum pressure for the MPPT in a scale-up PRO process. It is found that with OMC, the performance of the MPPT is improved significantly. Finally, a strategy to operate and coordinate the MPPT and OMC to deal with the rapid variations of the salinities are proposed and evaluated in terms of individual variation of the concentration or flow rate and co-variation of the both. The simulations demonstrate the preferred performance of the proposed strategy to adjust the operation subject to the rapid changes of the salinities.

Keywords: pressure retarded osmosis, maximum power point tracking, model-based control, salinity variation

1. Introduction

Osmotic energy, or salinity energy, from natural salinity gradients has been identified as a promising renewable energy source [1]. Compared to other renewable energy sources, it is less periodic and has no hazard operation. It is reported that 0.77 kWh (2.77 MJ) of energy is released from a mixture of a cubic meter of river water with seawater [2]. Therefore a massive annual discharge from river to ocean, ~37,300 km^3, represents a potentially enormous source of renewable energy generation that can significantly contribute to address global environmental and energy challenges of today and tomorrow [3]. Pressure retarded osmosis (PRO) is one of the most investigated technologies for extracting osmotic energy from natural salinity gradients. In a PRO osmotic power plant, two saline streams with different salinities flow at the two sides of a semi-permeable membrane. Draw solution is the high concentration saline stream and feed solution is the low concentration stream. Naturally, due to the non-zero solute difference across the membrane,

[1] Corresponding author: Tel: + 44 (0)20 7882 3774
E-mail address: m.h.shaheed@qmul.ac.uk

the water permeates from the feed side to the draw side. While, a hydraulic pressure that is lower than the osmotic pressure difference is applied on the draw solution to “retard” the water permeation and convert the osmotic energy into hydraulic energy. Thus, the energy generated from a PRO plant is harvested by expanding the pressurized permeation in a hydro turbine.

In recent years, membrane performance and process characteristics of PRO have been extensively investigated [4-10] and significant development in fabricating specific high performance PRO membrane has been achieved. In fact, this technology has been started to be utilized and tested in practice. In 2009, Statkraft, a Norwegian state-owned power company, opened the first PRO osmotic power plant and started to test the novel technology in real life [11]. In a scale-up PRO, the detrimental effects due to the draw concentration and the feed dilution are intensified. As a result, the efficiency of the entire membrane usage is significantly decreased that the average power density becomes lower than that obtained in a lab-scale PRO plant [12]. Actually, several investigations have been done to address the scale-up PRO performance and the optimum strategy of operation to maximize the salinity energy extraction. Because of the difficulty in constructing and operating a full-scale PRO plant to carry out experimental investigation, mathematical modelling based on the validated transport equations of PRO has become an important approach to study the scale-up process performance [13]. These studies focused on identifying the energy extraction limit and the detrimental effects of internal concentration polarization (ICP), external concentration polarization (ECP) and reverse solute permeation (RSP) on the performance of a scale-up PRO process [14, 15]. Feinberg et al first briefly validated the mathematical model of PRO using limited experimental results from [12]. Then, a comparison of the full-scale performance and operations between co-current PRO and RED in the salinity power generation was developed [16]. The results showed a significantly reduced performance of a scale-up PRO due to the detrimental effects and the increase of the process scale [16].

Recently, increasingly attention has been paid on PRO in order to further enhance the performance and push it to final practical application. Iso-watt diagrams for PRO performance evaluation was demonstrated by simulation, which can be used as aim in PRO membrane development [17]. In addition, novel configurations of PRO were studied in order to increase the overall efficiency of PRO. Altaee et al. carried out systematic investigations on modelling and optimization of dual-stage PRO process [18-21] and hybrid FO/RO/PRO process [22, 23]. Additionally, PRO showed promising power density in hybrid processes. In a novel PRO-MD (membrane distillation) hybrid process, according to the experimental results, the maximum power densities of 31.0 $W \cdot m^{-2}$ and 9.3 $W \cdot m^{-2}$ by the PRO using DI water and real wastewater mixing with 2M NaCl concentrate [24]. In another hybrid multi-stage vacuum MD and PRO process, maximum power density of 9.7 $W \cdot m^{-2}$ is achieved when river water is used as feed solution [25]. More recently, a preliminary investigation of hybrid solar and osmotic energy has been proposed and studied, the demonstrated benefiting improvements for both the PV and the PRO process especially push the osmotic power in the market of renewable energy generation [26].

On the basis of the clearer and deeper understanding of the process characteristics of the scale-up PRO process and significantly improved performance of PRO, real time operation and optimum control need to be considered. In fact, apart from the non-linear process characteristics of PRO, in realistic applications, disturbances, fluctuations and degradation of the components, process and environmental condition are also unavoidably affect the performance of osmotic energy generation. For example, due to the seasonal rainfalls, the concentration of both sea water and river water may fluctuate. It is reported that at a particular location in central San Joaquin Valley, the total dissolved

solids content deviated up to 52% from its annual average [27]. Temperature is another crucial influential environmental factor. Anastasio et al. evaluated water flux and power density in two temperatures (20 and 40 ^{0}C) and found the increased power densities with the increasing temperature and concentration [28]. Recently, Touati et al. carried out both theoretical and experimental investigations to address the effect of the operating temperature on hydrodynamics and membrane properties in PRO [29, 30]. In addition to the temperature effect, membrane properties may vary with respect to the hydraulic pressure on the draw solution due to the membrane deformation [31, 32]. Wan et al. tested a TFC membrane from 5 bar to 20 bar at an increment of 5 bar and found that the water permeability was at a constant 3.5 L/(m^2·bar·h) while the salt permeability increased monotonically from 0.28 L/(m^2·h) at 5 bar to 0.36 L/(m^2·h) at 20 bar [33]. Also in future as a stand-alone renewable energy generator or a part of hybrid energy generation, time-dependent strategy for bidding in market may need to change the PRO operation from state to state subject to the electricity price. In addition, the degradation of the membrane performance according to membrane fouling and the backwash and maintenance also affect the performance of the PRO salinity energy generation. Therefore, a maximum power point tracking (MPPT) control to extract maximum power from the PRO plant at each sample instant of real time becomes indispensable in salinity energy generation. However, to the horizon of the authors, there is no published work focusing on the MPPT of PRO or similar real-time control strategy subject to the variations of the operating conditions and salinities in the field.

Optimal control theory and its application have been important topics of research in renewable energy generation. With the increasing concern on global warming and environmental pollution, renewable energy plays an increasingly significant role in power generation. But because of the analytical solutions for complex systems are usually very difficult to obtain, the stable, robust and efficient MPPT systems represent a challenge for renewable energy designers. In last decades, several studies have been developed in tracking the maximum power point (MPP) for not only solar photovoltaic (PV) arrays [34-40] but also for fuel cell power plant [41, 42]. Conventional MPPT of PV arrays operated by sensing the current and voltage and the changing duty cycle of the converter to match the MPP. Aiming to achieve the same objective, widely implemented MPPT techniques differ markedly in terms of convergence speed, steady state oscillations and cost effectiveness [43], mainly including perturb and observe (P&O) [35, 36, 44] and incremental conductance (INC) [34, 45] which are most popular. In this context, in order to maximize the performance of PRO in practice, this work aims to fill the knowledge gap of MPPT in the field of the osmotic energy generation. Actually, operations and power output of a scale-up PRO is similar to PV arrays. Power output of both renewable energy generation are evaluated by the product of two variables which are the pressure and the flow rate of the permeation for PRO and the current and the voltage for PV arrays. With the increase on one variable, furthermore, another variable decreases in an operating generator. Therefore, MPPT techniques are potentially applicable in tracking the MPP of a scale-up PRO by sensing the flow rate and the pressure of the permeation.

This study aims to carry out an investigation on the development of MPPT controller for scale-up PRO osmotic power plant. First, the characteristics of the scale-up PRO plant is studied and the performance curve of flow rate and pressure ($\Delta V - \Delta P$) and curve of power output of pressure ($\overline{W} - \Delta P$) are investigated subject to different operational conditions and initial salinity conditions. Based on the process characteristics, two MPPT controllers based on P&O and INC-like algorithms are developed and tested by simulation. Furthermore, in order to improve the performance of the MPPT controllers, an optimum model-based controller is developed to select an appropriate initial

operating pressure. And a strategy to operate and coordinate the MPPT and an optimum model-based controller (OMC) subject to the rapid changes of the salinities is proposed. Finally, the improvements of the strategy are evaluated by simulations.

2. Characteristics of a scale-up PRO salinity power plant

A schematic diagram of a scale-up PRO process, as illustrated in Fig. 1, includes a boost pump (BP), a high-pressure pump (HP), an energy recovery device (ERD), an array PRO membrane module, and a hydro-turbine (HT). The mechanism of the PRO process in osmotic power generation can be found in our previous paper [6].

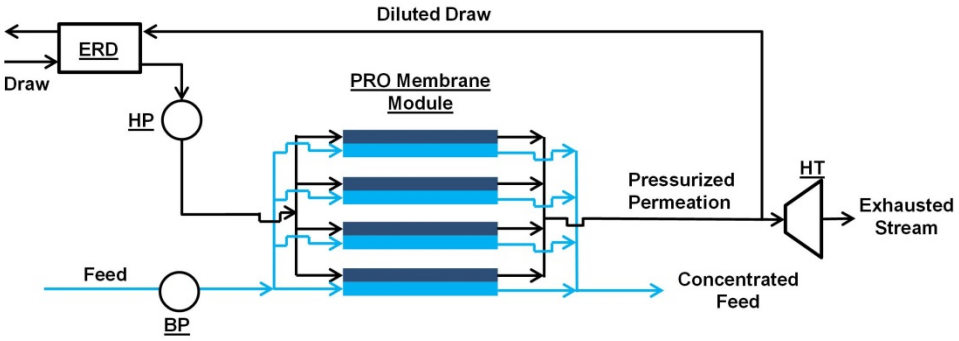

Fig. 1. Schematic diagram of a classical PRO osmotic power plant.

2.1. Mathematical model of PRO

In a PRO plant, the membrane power density is determined by the trans-membrane hydraulic pressure and the water permeation flux across the membrane [46] and the overall performance is evaluated by integrating the water flux and power density over the entire membrane used. The modelling framework of the scale-up PRO can be found in our previous work [47]. For a clear understanding, key equations describing a PRO process are listed in Table 1.

For a scale-up PRO process, the peak water flux occurs at the inlet of the membrane module. Due to the water permeation and reverse solute permeation, the draw dilutes and the feed concentrates rapidly along the flow channel. At a particular position along the membrane channel, the water flux and reverse solute flux are determined by the local concentration difference between the membrane surfaces and the membrane permeability-selectivity, which are represented by equations (T1) and (T2) in Table 1 incorporating the detrimental effects of ICP, ECP and RSP. Flow rates of the accumulative water permeation and reverse solution permeation can be obtained by integrating the water flux and salt flux as expressed by equations (T4) and (T5). Therefore, the concentration and flow rate of the draw and feed at each position in the flow channel can be updated by equations (T6), (T7), (T8) and (T9). In order to evaluate the overall efficiency of the osmotic energy extraction, specific energy extraction (SEE) is defined as shown in equation (T10). The SEE is the osmotic power output per initial feed solution for emphasizing the efficient utilization of the feed solution. For a PRO plant using natural salinity gradients, at coastal region, the low concentration stream (the feed solution), such as freshwater, river water and reclaimed water, is always limited compared to the enormous volume of seawater. Therefore, the efficiency of using

these water bodies should be optimized. Additionally, for a membrane process, overall membrane performance and efficiency are always concerns. Average power density (APD) of a scale-up PRO is expressed by equation T(11). On the basis of the equations T(10) and T(11), if the flow rate of the feed solution (V_F^0) and the membrane area (A_M) do not change, APD of a PRO is proportional to its SEE. In fact, either SEE or APD can be used as the MPP to be tracked using the MPPT controller to emphasize the efficiency of dilute solution or membrane. And if the initial flow rate of the feed solution and the membrane area are fixed, the tracked operation of the MPP of the APD and the SEE are same. In this study, APD is used to present the objective to design the MPPT controller.

TABLE 1

The steady-state model of the scale-up PRO process.

Physical quantity	Equation	NO#
Water Flux	..	(T1)
Reverse salt flux	$J_S = \mathrm{B}\left(\frac{c_D \exp(-J_W / k) - c_\mathrm{F} \exp(J_W S / D)}{1 + \frac{B}{J_W}(\exp(J_W S / D) - \exp(-J_W / k))}\right)$	(T2)
Power Density	$W = J_W \cdot \Delta P_{PRO}$	(T3)
Water Permeation	$d(\Delta V_P) = J_w d(A_m); \Delta q_P = \rho_P \Delta V_P$	(T4)
Reverse salt permeation	$d(\Delta V_S) = J_S d(A_m); \Delta m_S = \rho_S \Delta V_S$	(T5)
Concentration of the draw	$c_D = \frac{\mathrm{c}_D^0 q_D^0 - \Delta m_S}{q_D^0 + \Delta q_P}$	(T6)
Flow rate of the draw	$q_D = q_D^0 + \Delta q_P$	(T7)
Concentration of the feed	$c_F = \frac{\mathrm{c}_\mathrm{F}^0 q_F^0 + \Delta m_S}{q_F^0 - \Delta q_P}$	(T8)
Flow rate of the feed	$q_F = q_F^0 - \Delta q_P$	(T9)
Specific extractable energy (SEE)	$E = \Delta P_{PRO} \Delta V_P^* = \frac{\Delta P_{PRO} \Delta V_P}{V_F^0}$	(T10)
Average power density (APD)	$\overline{W} = \frac{E}{A_M}$	(T11)

2.2. $\Delta V - \Delta P$ and $\overline{W} - \Delta P$ characteristics

The non-linear nature of a PRO systems is apparent from its mathematical model. Also, the performance depends on a large number of influential factors, such as membrane performance, salinity conditions, process configuration, operating condition and efficiencies of components. The complex relationship between the membrane, operating condition and salinities results in highly non-linear permeation-pressure characteristics. In this section, the complex power output characteristics are studied in different conditions by simulation.

2.2.1. Membrane property

The permeability-selectivity trade-off relationship commonly exists and governs the separation membranes [48-50]. High permeability always results in low selectivity of the membrane. The trade-off relationship between permeability and selectivity of the thin film composite (TFC) polyamide membranes has been systematically investigated by Yip et al. [9]. According to their study, a trade-off relationship between the water and salt permeability coefficients of TFC polyamide membranes subject to chlorine-alkaline modification can be found. It indicates that with the increase on the membrane permeability, the loss of the selectivity is resulted in. Therefore, the high performance membrane corresponds to membrane having maximum water permeability, minimum solute permeability and minimum structural parameter. Several recent high performance membranes specifically for PRO have been found in literature and are listed in Table 2.

In Table 2, membranes, from M1 to M6, are fabricated membranes as reported in the recent literature and membrane M7 is a virtual membrane. The virtual membrane properties are assumed by Prante et al. to evaluate the membrane sensitivity on the overall performance of the PRO osmotic energy harvest for estimating the further improvement on the overall performance [51]. The virtual membrane, in fact, can be used to approximately identify the limiting performance with the ideal membrane.

The overall performance of a scale-up PRO plant with the membranes listed in Table 2 is evaluated by simulation. The results of the permeation and the APD of a PRO plant are shown in Fig. 2. All the parameters used in the simulations are listed in Table 3. In simulation, several assumptions are also used: i) osmotic pressure is considered to be linearly proportional to the concentration difference based on the modified van't Hoff law [52]. In the salinity range of 0-70 g/kg, the modified linear osmotic pressure approximation is validated and the maximum deviation is 6.8% [52, 53]; ii) constant hydraulic pressure difference in the membrane channel due to the negligible pressure loss; iii) mass flow rates are averaged in the cross-section area of the two flow channels; iv) membrane fouling and deformation do not occur; v) For simplicity, a constant density of the water is used for both draw and feed solutions [54].

The results shown in Fig. 2, clearly indicates that the membrane properties have a significant influence on $\Delta V - \Delta P$ and $\overline{W} - \Delta P$ characteristics of PRO. The specific influence on the PRO process with respect to the membrane permeability, selectivity or structural parameter is not the topic of this study and it can be found in previous literature focusing on the high performance membrane development [9]. Conversely, on the basis of their work, membranes with different membrane permeability-selectivity and structural parameter result in the variations on both the permeation and the overall performance of the PRO process.

TABLE 2
Selected membrane properties from recent publications.

NO	Publications	A [L/(m^2·bar·h)]	B [L/(m^2·h)]	S [μm]
M1	Chen et al. (2015) [55]	2.5	0.9	405
M2	Kim et al. (2015) [56]	3.12	0.55	1022
M3	Achilli et al. (2014) [31]	5.11	0.087	310
M4	Han et al. (2014) [57]	4.3	0.47	640
M5	Song et al. (2013) [58]	4.1	1.74	150
M6	Chou et al. (2012) [59]	3.32	0.14	460
M7	Prante et al. (2014) [51]	67.32	0.04	6.87

TABLE 3
Parameters used in the simulations of the PRO.

Parameter	Value
Concentration of the draw solution	35 g/kg
Concentration of the feed solution	0.1 g/kg
Dimensionless flow rate	0.5
Temperature	298 K
Mass transfer coefficient	138.6 L $m^{-2}h^{-1}$ [9]
Diffusion coefficient	1.49×10^{-9} m^2 s^{-1} [60]
Density of the solutions	1,000 kg m^{-3}
Modified van't Hoff coefficient	0.7307 bar kg g^{-1} [52]
Specific membrane area	0.1 m^2 per 1 L/h feed solution
Efficiency of the HP, ERD and HT	70%, 95% and 90%

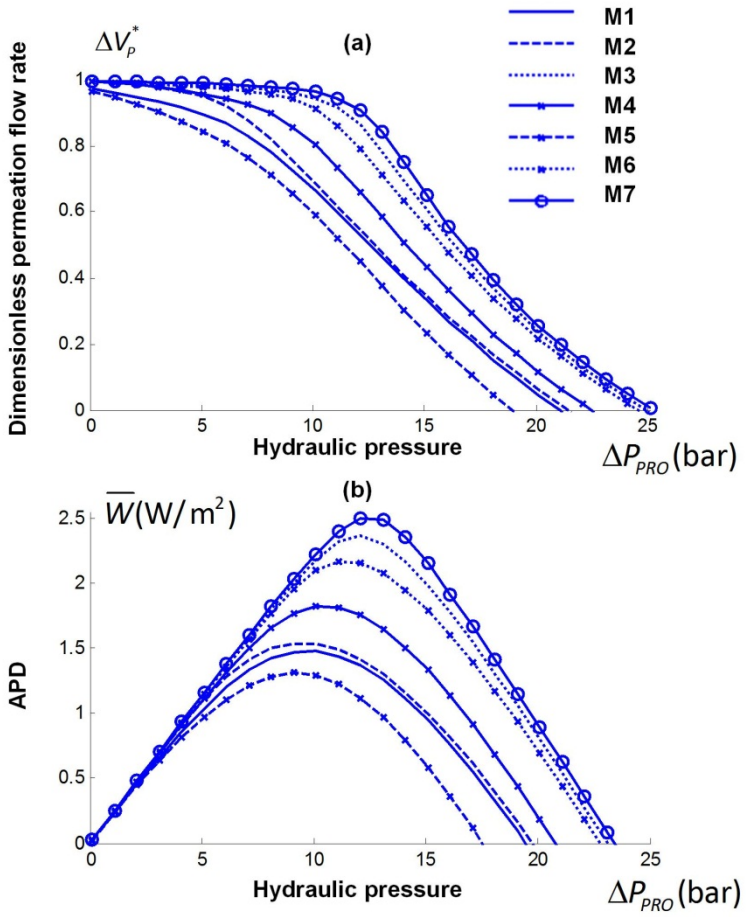

Fig. 2. The permeation-pressure ($\Delta V_P^* - \Delta P$) and the APD-pressure ($\overline{W} - \Delta P$) characteristic curves of the PRO plant subject to different membrane properties

2.2.2. *Concentrations* of salinity and dimensionless flow rate

Due to the seasonal rainfalls, the concentration and flow rate of the natural salinities may fluctuate both for seawater and river water. The example in the central San Joaquin Valley indicates significant fluctuations of the concentration [27]. In addition, for hybrid RO-PRO plant, if the brine from RO is used as the draw solution for PRO, the concentration of the draw is determined by the operation of RO. With different water recovery ratio achieved in RO, the brine with different concentration and flow rate flows into PRO. Similarly, due to the seasonal rainfalls and the changes in the salinities source, the available volumes of the two salinity gradients may change.

These variations in concentration and flow rate of the salinities result in the changes of the performance of the PRO, which is shown in Fig. 3. In Fig. 3(a) and 3(b), four dimensionless flow rates are selected for different flow rates from the low to the high dimensionless flow rate. And in Fig. 3(c) and 3(d), three salinities are chosen, representing the seawater to the concentrated brine. The results clearly indicate the influences of the salinities on the performance of the PRO process. However, a MPP can be found in each condition demonstrated in Fig. 3(b) and 3(d).

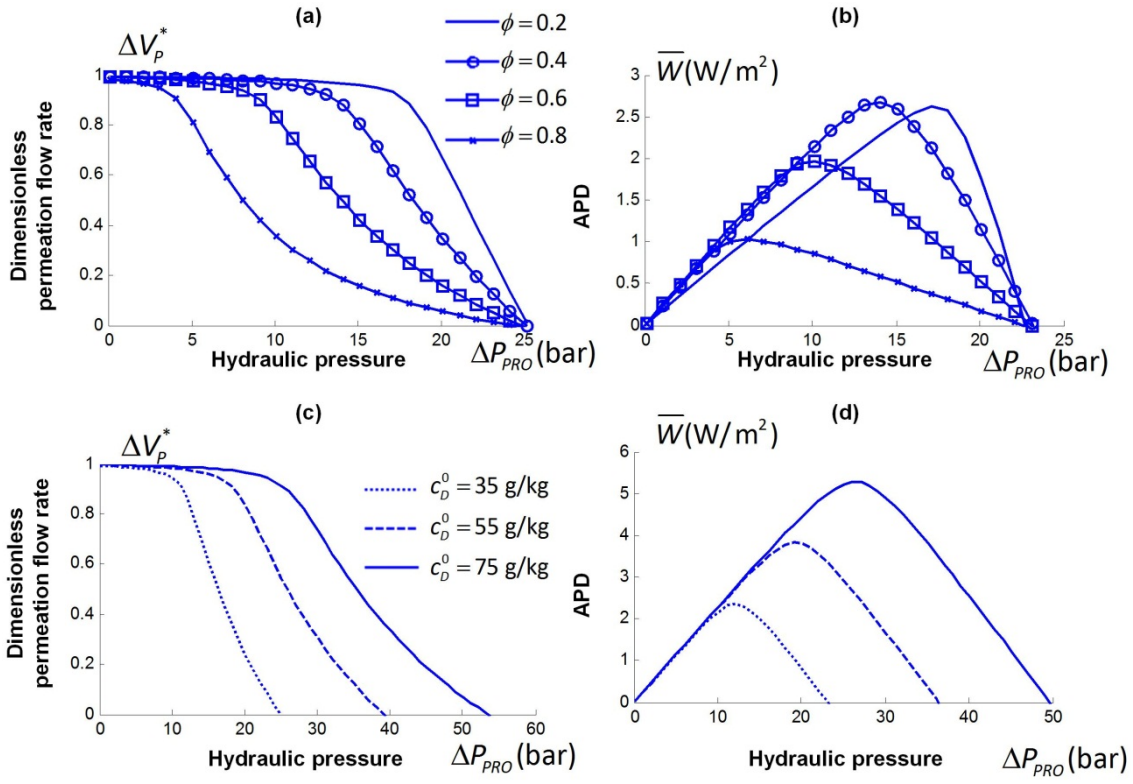

Fig. 3. The permeation-pressure ($\Delta V_P^* - \Delta P$) and the APD-pressure ($\overline{W} - \Delta P$) characteristic curves of the PRO plant subject to different concentration and flow rate of the salinities.

3. MPPT for PRO

As shown in Section 2, many influential factors affect the osmotic energy extraction of the PRO process. The aim of employing MPPT is to ensure that at any operational condition, maximum power is extracted from the PRO plant. Similar to the conventional MPPT of solar PV that operates by sensing the current and voltage, MPPT of a PRO is achieved by changing the applied pressure on the

draw solution based on the measurement of the osmotic power output. An illustrated diagram of the MPPT controller is shown in Fig. 4. The MPPT evaluates the osmotic power generated by the HT and adjust the applied hydraulic pressure on the draw solution. The pressure transition can be achieved using the variable frequency drive to change the speed of the HP [61]. This study aims to investigate the MPPT performance by simulation. Thus, at the early stage, the algorithm of the MPPT is considered with the available measured osmotic power output. And the targeted pressure can be actuated on the draw solution by a fast and stable controller.

In this investigation, two general methods, P&O and incremental mass-resistance (IMR), are applied for the MPPT of PRO. These two methods are extensively utilized in MPPT of solar PV in which IMR is an INC-like method. They can be classified into online methods, also known as model-free methods, in which, usually, the instantaneous values of measured variable are used to generate control signals.

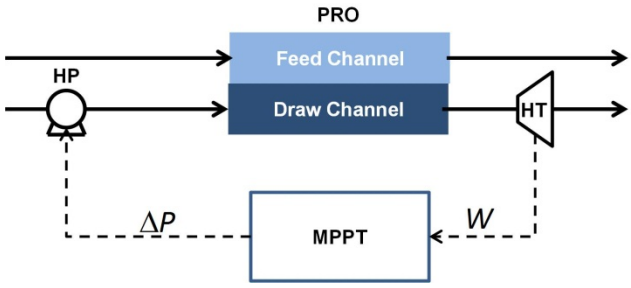

Fig. 4. Schematic diagram of MPPT in PRO.

3.1. Perturb & observe (P&O) method

P&O can be implemented by applying perturbation to the reference hydraulic pressure applied on the draw solution. A flowchart illustrating this method is depicted in Fig. 5, where pressure is the reference signal. Therefore, the goal of this algorithm involves pushing the reference pressure signal towards MPP thereby causing the instantaneous pressure to track the MPP. As a result, the output power will approach MPP. To this end, a small but constant perturbation is applied to the hydraulic pressure, which is “C” in the flowchart.

The hydraulic pressure is changed by applying a series of small and constant perturbations denoted by (C=ΔP) on a step-by-step basis in order to change the operating point of the PRO process. Following each perturbation, the output osmotic power variation (ΔW) is measured. If ΔW is positive, osmotic power will approach the MPP, therefore, a hydraulic pressure perturbation of the same sign must be applied in the following stage. A negative ΔW, on the other hand, implies that osmotic power has shifted away from the MPP, and a perturbation of opposite sign will have to be applied. This repeating process is stopped until the MPP is reached.

The MPPT using P&O algorithm has two main drawbacks. First, the selection of the perturbation applied to the system determines the oscillations as well as the convergence of the tracking. Larger perturbation results in faster tracking MPP but with larger oscillation as well. If the applied perturbation is too small, on the other hand, the oscillation around MPP will be reduced, but the rate of the convergence reduces. Therefore, inherent trade-off between the oscillation and the response rate exists in this algorithm. In addition, P&O is prone to tracking errors if the operating point changes quickly.

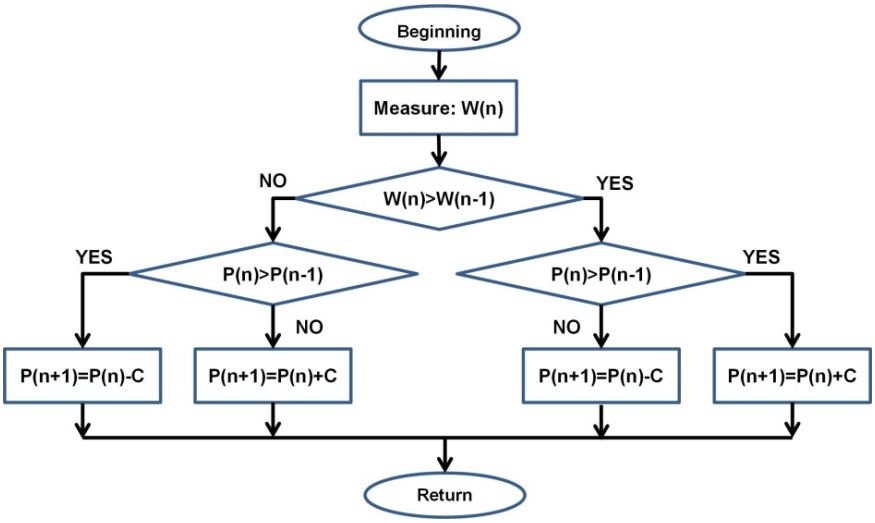

Fig. 5. Flowchart of MPPT using P&O algorithm.

3.2. Incremental mass-resistance (IMR) method

The INC method in MPPT of PV employs the slop of the PV array power characteristics to track MPP. Similarly, in PRO, this method is also on the basis of the fact that the slope of the $\overline{W}-\Delta P$ curve is zero at the MPP, positive for values of the APD smaller than the MPP, and negative for values of the APD greater than the MPP.

An illustration of the IMR algorithm is shown in Fig. 6. The maximum APD, $\overline{W}_{MPP}=\dfrac{\Delta P_{MPP}\Delta V_{MPP}}{A_M}$, is achieved by differentiating the APD with respect to hydraulic pressure and setting the result to zero, which is $d\overline{W}/dP=0$. Accordingly, when the membrane area is fixed, the relation of the deviations of the pressure and the permeation can be obtained, which is

$$dV/dP\cong\Delta V/\Delta P=-V_{MPP}/P_{MPP} \qquad \text{at MPP when } d\overline{W}/dP=0 \tag{1}$$

As shown in Fig. 6, the curve is divided into three parts including left of the MPP where $dV/dP>0$, MPP where $dV/dP=0$ and right of MPP where $dV/dP<0$. Therefore, by evaluating the derivative one can test whether the PRO is operating at or near or far away from the MPP. The strategy of the evaluation is shown below,

$$\begin{aligned} dV/dP=0 &\longrightarrow \Delta V/\Delta P=-V/P \longrightarrow \text{At MPP} \\ dV/dP>0 &\longrightarrow \Delta V/\Delta P>-V/P \longrightarrow \text{Left of MPP} \\ dV/dP<0 &\longrightarrow \Delta V/\Delta P<-V/P \longrightarrow \text{Right of MPP} \end{aligned} \tag{2}$$

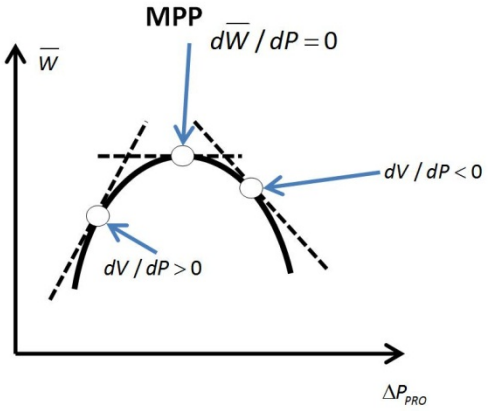

Fig. 6 An illustration of IMR algorithm in $\overline{W}-\Delta P$ curve.

In the INC method, the conductance of the PV array is represented by "I/V". Compared to that, a similar concept of "mass-resistance" is defined as "V/P" and used in the MPPT of PRO. As a result, the MPP can be tracked by comparing the instantaneous mass-resistance ("V/P") to incremental mass-resistance ($\Delta V/\Delta P$) as shown in Fig. 7. And it is proposed to call the method incremental mass-resistance method. In Fig. 7, the hydraulic pressure is the reference variable at which the PRO is ensured to operate. At the MPP, referencing pressure equals to P_{MPP}. In the algorithm, a parameter ε_{IMR} is used to control the tolerance of the convergence. The large tolerance results in mitigated oscillation. Once the MPP is reached, the operation of the PRO is maintained at this point unless a change in permeation occurs as a result of a change in operating condition leading to MPP transition. The algorithm, then, tracks the MPP by applying decrement or increment. A constant deviation of the referencing pressure is illustrated in Fig. 7. Therefore, fast tracking can be achieved by applying larger increments, but the system may not operate stably at the MPP and oscillation around the MPP may be resulted in. Similar trade-off between the convergence speed and the oscillation is also involved in IMR.

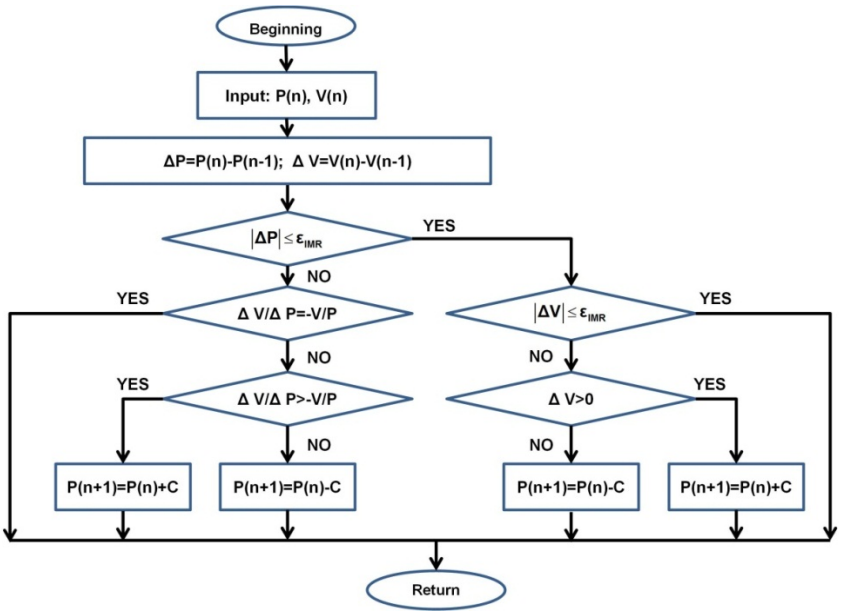

Fig. 7. Flowchart of IMR algorithm.

3.3. Simulation and results

The two methods, P&O and IMR, are tested in MPPT of a PRO process by simulation. MPPT aims to track the MPP without any information of the PRO plant. The initial pressure is set to be 1 bar. And several step-sizes of the perturbation and increment are studied. The MPPT applies the initial hydraulic pressure on the draw solution, and adjusts the pressure depending on the measured osmotic power output. As shown in Fig. 4, the performance of the PRO plant is obtained by simulation on the basis of the model shown in Table 1. Membrane M3 is selected for the simulation of the PRO plant because of its high performance. And other parameters are same to the parameters listed in Table 3.

The results of the osmotic power output with MPPT using P&O and IMR are presented in Fig. 8. Three step-sizes of the perturbation and pressure increment, 2, 1 and 0.5 bar, are studied and the results are presented in Fig. 8(a), 8(b) and 8(c), respectively. For the IMR methods using the three increments, the values of ε_{IMR} are set as 1×10^{-2}, 1×10^{-2} and 1×10^{-3}, respectively. The results in literature suggested that the transition from one steady state to another steady state for RO process changes in different process scales. Bartman et al. changed the flow rate within a wide range of operation less than ~1 min in UCLA experimental RO membrane water desalination system [62]. Sassi et al. pointed out that pseudo steady-state model of RO can be assumed for time steps more than 0.25 h [63]. For PRO, no literature studying the transition between the operations is reported. But due to the inherent similarity to RO desalination plant, the range of the transition time can be estimated. In this study, a general sample instant is used for representing the sensing period at the early stage.

The results clearly indicate that the performance of both the methods is parameter dependent. With the larger step-size of the perturbation and increment, a faster convergence of the MPPT is achieved. In Fig. 8(a), both the MPPT approach near to MPP within 10 sample instants. In contrast, for finer step-sizes, 1 and 0.5 bar, the required numbers of sample instants to near the MPP are approximately 10 and 20, respectively. Furthermore, comparing the results of P&O and IMR, it is found that the convergence of IMR is better than P&O. The oscillations in all the three tested cases are significantly mitigated compared to the results of P&O. In this study, P&O method has only one manipulated parameter, perturbation on pressure, to control the MPPT. The oscillation of the PRO plant close to the MPP increases when the perturbation of the hydraulic pressure is large. As shown in Fig. 8, from (a) to (c), the oscillation reduces significantly with the decrease on the perturbation. In contrast, two parameters, increment and parameter ε_{IMR}, are used in IMR to control the performance. The parameter ε_{IMR} changes the tolerance of the convergence and manipulates the oscillation. The control of the convergence makes the IMR flexible in MPPT. If a particular deviation of the MPP is acceptable, the stability of the MPPT might be improved by adjusting the parameter ε_{IMR}.

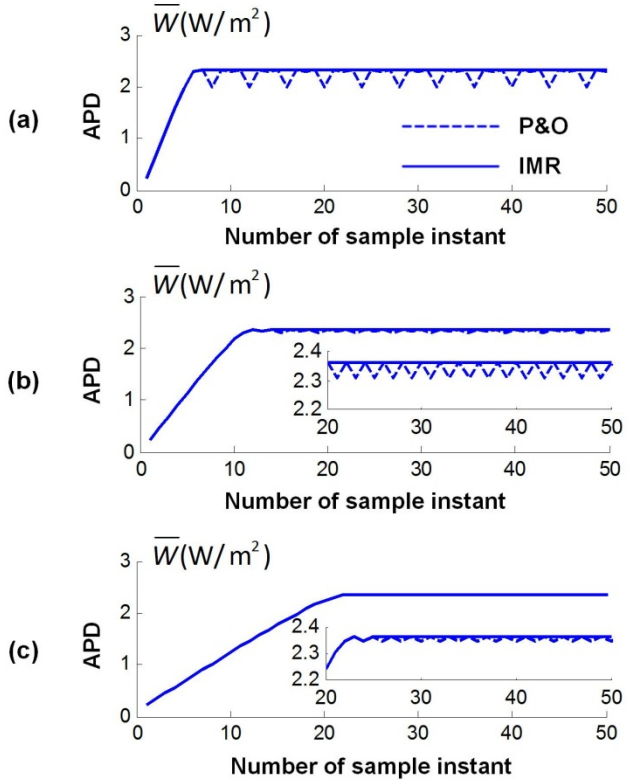

Fig. 8. Osmotic power output with MPPT using P&O and IMR.

In fact, the fluctuation of the temperature affects the permeability and selectivity of the membrane [29]. Anastasio et al. reported that the permeability coefficients of water and solute increase from 0.589 L/(m^2·bar·h) and 0.319 L/(m^2·h) to 1.12 L/(m^2·bar·h) and 0.580 L/(m^2·h) respectively, when the temperature of the draw solution increases from 20 ^{0}C to 40 ^{0}C [28]. Consequently, the MPP of PRO is also varied with respect to the change of the operating temperature. At present, there is no explicit model or theory to address and predict the temperature effect on the performance of PRO plant, which makes it difficult to study the transitions between the possible MPP considering the varying operating temperature. However, the proposed MPPT controller, both P&O and IMR, are generic and model-free methods. Therefore, these controllers are capable of capturing the changing MPP with respect to the variation of the operating temperature.

As the mechanism of the temperature effect on the hydrodynamics and membrane parameters is beyond the scope of this study, both the MPPT controllers are tested using the discrete parameters of the solution characteristics, hydrodynamics and membrane properties, which represent the varied operating conditions due to the changing temperature (also verification of the MPPT controller to deal with the varying membrane properties for several cases with deformed membrane subject to applied pressure changes). These parameters are from Ref [30] and shown in Table 4 in which ICP factor represents the ICP effect in the support layer. It can be used to estimate the varied structure parameter of the membrane using diffusion coefficient. It should be noted that the parameters listed in Table 4 are usually case-dependent, which are determined by many factors, such as geometry of the membrane module, membrane area, concentration, velocity, temperature and etc. This study aims to demonstrate the capability of the MPPT controller to capture the changing MPP when the properties of the solution and membrane are varied due to temperature.

TABLE 4 Varied parameters of solution characteristics and hydrodynamics and membrane properties [30]. The draw solution studied is 35 g/kg (0.6 M approximately) NaCl solution.

Temperature (^{0}C)	A ($m \cdot s^{-1} \cdot Pa^{-1}$)	B ($m \cdot s^{-1}$)	D ($m^2 \cdot s^{-1}$)	k ($m \cdot s^{-1}$)	ICP factor, S/D ($m^{-1} \cdot s^1$)
20	1.06×10^{-12}	2.62×10^{-8}	3.50×10^{-9}	4.27×10^{-4}	1.32×10^{6}
30	1.43×10^{-12}	4.25×10^{-8}	4.54×10^{-9}	9.74×10^{-4}	1.00×10^{6}
40	1.74×10^{-12}	5.87×10^{-8}	5.74×10^{-9}	10.88×10^{-4}	0.82×10^{6}
50	1.98×10^{-12}	8.00×10^{-8}	7.09×10^{-9}	11.98×10^{-4}	0.71×10^{6}

The results are shown in Fig. 9 in which both the MPPT controllers are studied for tracking the MPP operated at four different temperatures, namely 20, 30, 40 and 50 ^{0}C. The varied performance of the PRO plant is simulated using the model shown in Table 1 and the varied parameters are listed in Table 4. The perturbation pressure is 1 bar for both MPPT controllers. In the simulations, the temperature effect on the osmotic pressure is not considered. The osmotic pressure is estimated by the modified van't Hoff's law. The results shown in Fig. 9, clearly verifies both MPPT controllers to track the varied MPP with respect to different operating temperatures. Both the P&O and IMR algorithms successfully identify the changing operations due to the transiting temperature and perturb the pressure to track the varied MPP. Furthermore, comparing the two algorithms, oscillation of the APD is found using P&O algorithm in all operations and IMR shows better performance in terms of tracking the trajectory according to its lower oscillation. The manipulated parameter ε_{IMR} is set as 0.02 in this case.

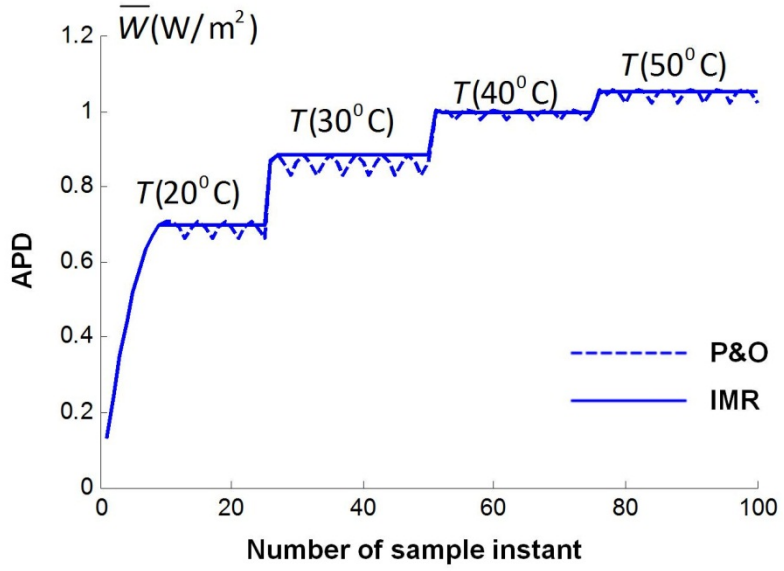

Fig. 9 Osmotic power output with MPPT using P&O and IMR subject to changing operating temperature.

In addition, both the methods have advantages of low cost, independence of the PRO plant, easy implementation, stable and robust performance. Based on the experiences of MPPT using P&O and INC in PV array, both the methods are most commonly used and easy to implement. P&O method can be implemented using either an analogue circuit or a digital circuit and INC is commonly implemented using a digit circuit. These experiences can be extensively used in MPPT of PRO using

P&O and IMR. Also, for PV array, rapid changes of the solar irradiation and temperature cause the MPP transitions fast and periodic. However, the changes in PRO may be more gradual compared to solar PV. The properties of membrane change in a continuous and gradual way due to deformation and fouling. The permeability and selectivity of the membrane commonly decrease monotonically with respect to time, resulting in the new optimum MPP may still in the vicinity of the previous MPP. Therefore, the two robust and simple methods will be less susceptible to confusion by system dynamics in MPPT of PRO with respect to membrane performance degradation.

4. An optimum model-based controller (OMC)

Compared to the PV array, the PRO process needs more time to achieve the transition from one steady-state to another steady-state. Therefore, in order to achieve a fast response of the MPPT to the changes of intentional operations and transitions, such as the change of flow rate or change of the solutions, improvement of the controller is needed. From the experiences of MPPT in PV array, adaptive and variable step-size in P&O and INC have been used. An adaptive strategy is achieved by using a parameter or several parameters to change the step-size of the perturbation or increment according to the change of the measurements. Manual tuning of the parameter(s) is tedious and the obtained optimal results may be valid only for a given system and operating condition [37]. It means that with the changing operating environments, a constant pre-optimized parameter may fail to track the MPP efficiently. In this study, an optimum model-based controller (OMC) is used to determine the initial optimum hydraulic pressure with several operating variables of the PRO plant.

4.1. Development of OMC

In a PRO plant without considering CP or RSP, the optimum hydraulic pressures to achieve the peak power density of a coupon scale PRO and the maximum SEE of a full scale PRO have been investigated by Yip et al. [2]. According to their study, on the basis of the parameters and assumptions in this study, the optimum pressures can be represented as,

$$\begin{aligned} \Delta P_{IPRO}^{PD} &= \frac{1}{2}(C_{OS}(c_D^0 - c_F^0)); \\ \Delta P_{IPRO}^{SEE} &= C_{os}[(1-\phi)c_D^0 - \phi c_F^0 + (2\phi - 1)\sqrt{c_D^0 c_F^0}] \end{aligned} \tag{3}$$

where ΔP_{IPRO}^{PD} and ΔP_{IPRO}^{SEE} represent the optimum pressure to achieve the peak power density and optimum SEE in an ideal PRO process with no CP or RSP. The subscript IPRO denotes the ideal PRO process with no CP or RSP. The pressure for the peak power density is the optimum theoretical pressure for the membrane unit at inlet. And the pressure for the maximum SEE is based on the full-scale PRO process in which the net driving force is zero at outlet. In fact, these two pressures can be used to be the initial pressure for the MPPT. For a full scale PRO process, if the membrane area does not change, the maximum SEE results in maximum APD. In a coupon-scale PRO, selecting ΔP_{PRO}^{PD} for the initial pressure is better, and ΔP_{PRO}^{SEE} is better for a large scale PRO which is close to achieve full-scale PRO discharge. But the optimum pressure is not proportional to the process scale due to the non-linearity of the process dynamics.

However, for a PRO plant considering CP and RSP effects, the optimum pressures may deviate from the theoretical pressure represented by equation (3). In order to find the optimum pressure further close to the realistic pressure, the OMC is further improved. Previous studies have already carried out works on identifying the optimum operating pressures numerically with respect to the detrimental effects in a scale-up PRO [15, 33]. For a hydraulic pressure to achieve the peak power density considering CP and RSP effects, the optimum pressure can be quickly found by numerical analysis. But for the optimum pressure of the APD for a scale-up PRO, the calculation is more tedious considering the scale of the membrane utilization, because the evaluation of each PRO operation needs to integrate all the water flux along the flow channel, which is time consuming for on-line control.

In this study, therefore, an approximation of the optimum pressure of the SEE considering CP and RSP in a scale-up process is proposed. For a stable high-performance membrane, the membrane permeability, selectivity and structural parameter are assumed to be not varied significantly. The accumulative CP and RSP effects gradually and continuously affect the scale-up PRO performance. And these detrimental effects do not significantly change the relationship between the membrane-unit scale operation and the full-scale process operation. Based on these assumptions, thus, the optimum pressure of the full-scale PRO process considering CP and RSP can be estimated in terms of the membrane unit performance and the theoretical full-sale process dynamics. An approximation of the two pressures in the ideal PRO and PRO considering CP and RSP is represented as

$$\frac{\Delta P_{DPRO}^{SEE}}{\Delta P_{DPRO}^{PD}} \cong \frac{\Delta P_{IPRO}^{SEE}}{\Delta P_{IPRO}^{PD}} \tag{4}$$

where the subscript DPRO denotes the PRO process considering detrimental CP and RSP effects. Therefore, the approximation of the pressure to achieve the maximum APD and SEE in a full-scale PRO considering CP and RSP can be derived as,

$$\Delta P_{DPRO}^{SEE} = \frac{\Delta P_{IPRO}^{SEE}}{\Delta P_{IPRO}^{PD}} \Delta P_{DPRO}^{PD} \tag{5}$$

The approximated pressure derived in equation (5) can be used as one of the candidates for the initial pressure setting of the MPPT controllers to address the detrimental effects of CP and RSP. The schematic diagram of the PRO plant with MPPT and OMC is illustrated in Fig. 10. The OMC senses the initial flow rates and concentrations of the draw and the feed solution, and determines the initial pressure for the MPPT based on the pre-measured membrane properties, A B and S. Then, the MPPT using P&O or IMR algorithm tracks the MPP locally around the estimated optimum pressure with a small step-size of the perturbation or increment.

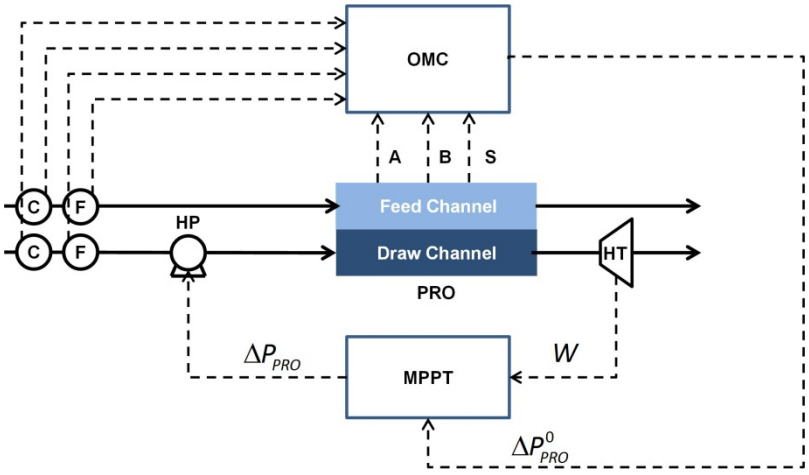

Fig. 10. Schematic diagram of the PRO plant using MPPT and OMC.

4.2. Simulation of MPPT and OMC

Therefore, in this section, a series of simulation are developed to evaluate the performance of the osmotic power output tracking by using MPPT and OMC. Two step-sizes of MPPT using P&O and IMR, 0.5 and 0.1 bar, are used. Two models of OMC for the initial optimum hydraulic pressure, IPRO and DPRO which are represented by equations (3) and (5), respectively, are also compared by simulation. Membrane M3 is selected for the simulations of the PRO plant. And other parameters are same as the parameters listed in Table 3. For consistency with the simulation based on the same step-size in Section 3.3, the parameter ε_{IMR} is set to be 1×10^{-3} (the same parameter for the step-size 0.5 bar of IMR in Section 3.3) for all the MPPT using IMR algorithm.

The results are shown in Fig. 11 in which osmotic power output with OMC and MPPT using P&O algorithm are presented in (a) and (c), and that with OMC and MPPT using IMR algorithm are plotted in (b) and (d). In addition, in (a) and (b), the step-size of the perturbation and increment is 0.5 bar and the step-size is 0.1 bar in (c) and (d).

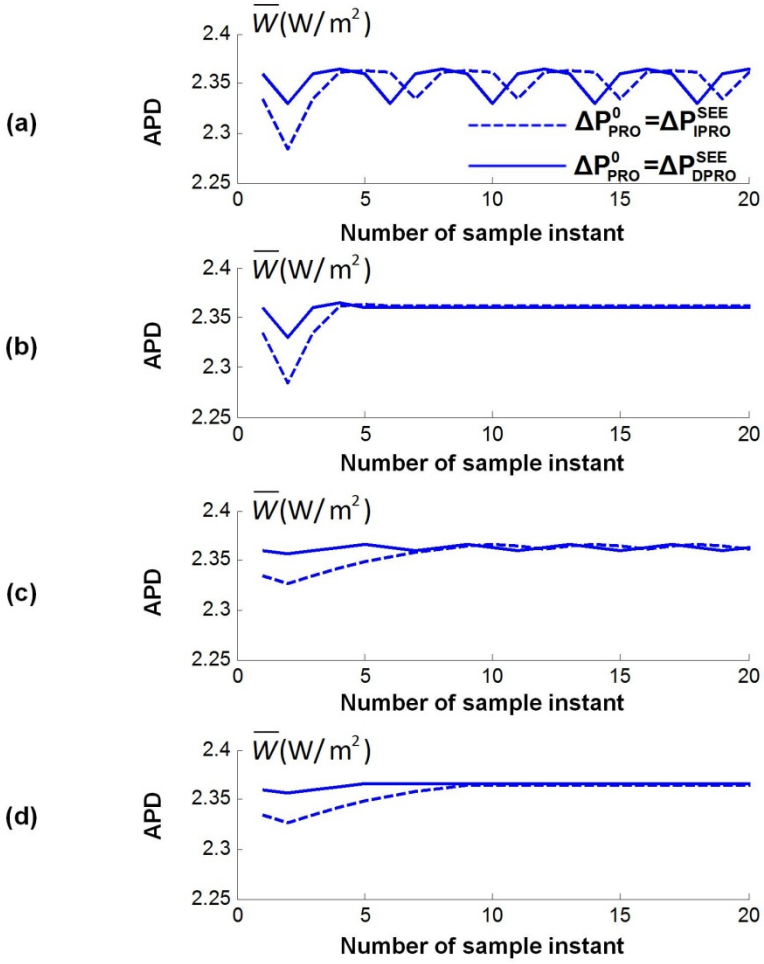

Fig. 11. Osmotic power output with MPPT using P&O and IMR and OMC using equation (3) and equation (5).

First, the results indicate that the rise time of the MPPT is significantly reduced by using the OMC. With the step-size of 0.5 bar for the perturbation or incremental pressure, as shown in Fig. 8, the MPPT without OMC makes the PRO approach to its MPP more than 20 sample instants. In contrast, MPPT with OMC takes less than five sample instants for both algorithms. Moreover, the fast response time also allows the MPPT applying a finer step-size to reduce the oscillation of the power output using P&O algorithm. As shown in Fig. 11(c), the oscillation caused by P&O algorithm is considerably reduced by using 0.1 bar perturbation pressure and the rise time is still much quicker compared to the MPPT without OMC. In addition, the two models of OMC, IPRO and DPRO, show different performance of the MPPT. The results clearly indicate that the pressure estimated based on DPRO-OMC is closer to the MPP, and hence, a fast tracking is observed. As results shown in Fig. 11, quicker tracking of OMC using estimated optimum pressure based on DPRO is found. Therefore, MPPT with DPRO-OMC is capable to employ a finer step-size to mitigate the oscillation around the MPP.

In fact, the combination of the OMC and MPPT is efficient and robust to track the MPP of the PRO process. The OMC is a model-based controller to estimate the optimum operating pressure for the PRO process based on the measured data and set the initial pressure for the MPPT controller to improve the convergence. In addition, a generalized OMC can be used as a pre-treatment for the MPPT in applications. For different PRO processes, different model can be used to estimate the initial pressure. Therefore, the OMC aims to improve the performance by the knowledge of the

process, which is efficient. In contrast, the MPPT is a general and robust method that is used to deal with the non-linear characteristics of the PRO and possible fluctuations.

4.3. Variations of flow rate and concentration of salinities

Furthermore, with the knowledge and information of the PRO plant, implementation of an OMC makes the PRO plant able to adjust the operation according to the rapid changes of the salinities. The combination of the OMC and MPPT is capable to respond quickly for the change of the concentration and flow rate of the salinities. A strategy to deal with these fluctuations is proposed based on the developed OMC and MPPT. The flowchart illustrating the strategy is shown in Fig. 12. The MPPT operates starting at the optimum pressure estimated by the OMC. For tracking of the MPP with respect to the variations of the flow rate and concentration of the salinities, at the sample instant n, the estimated optimum pressure by OMC, $\Delta P_{PRO}^{SEE}(\mathrm{n})$, is compared to the potential current applied pressure applied by MPPT, $\Delta P_{PRO}(\mathrm{n})$. If the estimated pressure is close to the current applied pressure in which the vicinity can be controlled by the parameter ε_{OMC}^{1}, the pressure $\Delta P_{PRO}(\mathrm{n})$ is applied on the draw solution and the MPPT works around the current applied pressure. Conversely, if the estimated pressure deviates from the pre-defined vicinity of the current applied pressure, the decision is made based on the comparison between the current estimated optimum pressure and previous optimum pressure, $\Delta P_{PRO}^{SEE}(\mathrm{n}-1)$. If the current optimum pressure is close to the previous estimated pressure based on the parameter ε_{OMC}^{2}, the pressure $\Delta P_{PRO}(\mathrm{n})$ is applied on the draw solution and the MPPT works around the current applied pressure. Otherwise, the current pressure for the MPPT is set to be the current estimated pressure and is adjusted around the current estimated pressure by OMC.

These two parameters, ε_{OMC}^{1} and ε_{OMC}^{2}, are used to control the performance and cooperation between the MPPT and the OMC to deal with the rapid change of the environment and operating condition. As discussed above, the combination of OMC and MPPT provide efficient and robust solution to deal with the possible fluctuations. Due to the “imperfect” mathematical model of the PRO process, the selection of parameter ε_{OMC}^{1} allows the MPPT searching for and tracking the real MPP around the modelled MPP based on the OMC. In addition, another parameter ε_{OMC}^{2} aims to identify the rapid and significant change of the environment or/and operating condition.

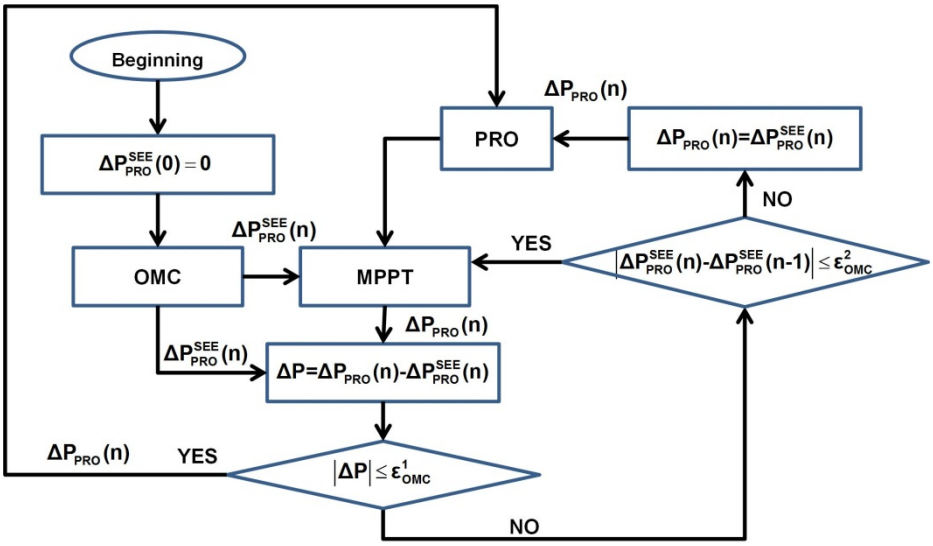

Fig. 12, Flowchart of the strategy to operate MPPT and OMC subject to the variations of the flow rates and concentrations of the salinities.

For the purpose of illustration of the proposed strategy of MPPT using OMC to deal with the variations of the salinities, two simple salinities fluctuation profiles of both the flow rate and concentration are shown in Fig. 13. Specifically, we consider a 50 sample instants time window in which the dimensionless flow rate is used. For the first 25 sample instant, the dimensionless flow rate is 0.5, and then the dimensionless flow rate is jumped to 0.8 for the remaining 25 sample instant. For variations of the concentration, the draw concentration for the first 15 sample instants is 35 g/kg, increases to 55 g/kg from the 16th to the 35th sample instant, and then is reduced to 35 g/kg for the remaining 15 sample instants. Three case studies are carried out to evaluate the performance of the MPPT with OMC, including the individual variation of the flow rate of the draw, individual variation of the draw concentration, and the co-variations of the both flow rate and concentration. It is important to point out that the proposed strategy and associated analysis can be readily extended to deal with more complex salinities fluctuations profiles.

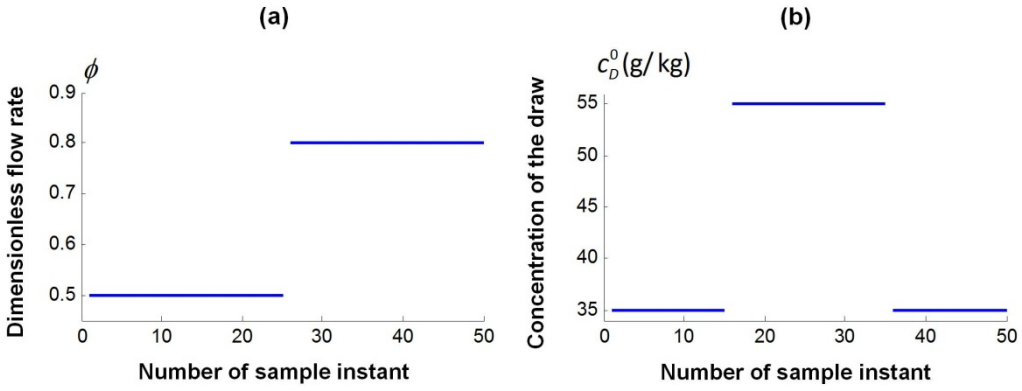

Fig. 13 . Variations of the concentration and flow rate of the salinities.

The results, shown in Fig. 11, show very small oscillation of the osmotic power output around the MPP both algorithms compared to the large variation of the salinities as shown in Fig. 8. Both

the algorithms have very high performance. Therefore, for simplicity, only MPPT using P&O is considered in this section. First the performance of the MPPT with OMC is evaluated by dealing with variation of the flow rate of the draw. The results are shown in Fig. 14 in which two strategies are evaluated. One is the simple combination of MPPT and OMC, in which OMC just provides the initial optimum pressure at the beginning and then the MPPT with P&O algorithm tracks the MPP. We call it SIM-MPPT-OMC strategy. Conversely, another is the optimum strategy illustrated in Fig. 12. We call it OPT-MPPT-OMC strategy. In the simulation, 0.1 bar is selected for the perturbation pressure in OPT-MPPT-OMC, and two step-sizes, 0.1 and 0.5 bar, are studied for the perturbation pressure in SIM-MPPT-OMC. ε_{OMC}^{1} is set as ten times of the perturbation pressure and ε_{OMC}^{2} is set as 2 bar. The results clearly show the rapid response of the OPT-MPPT-OMC to track the changes of the flow rate of the draw solution and resulting varied osmotic power output. Compared to the SIM-MPPT-OMC strategy with two different step-sizes, the OPT-MPPT-OMC has fast tracking and small oscillation when the flow rate of the draw is suddenly changed. For SIM-MPPT-OMC, the trade-off of the rise time and the oscillation still exists. Larger step-size tacks the change fast but with a large oscillation around the MPP. In contrast, implementation of the small step-size results in long time-period to reach the MPP.

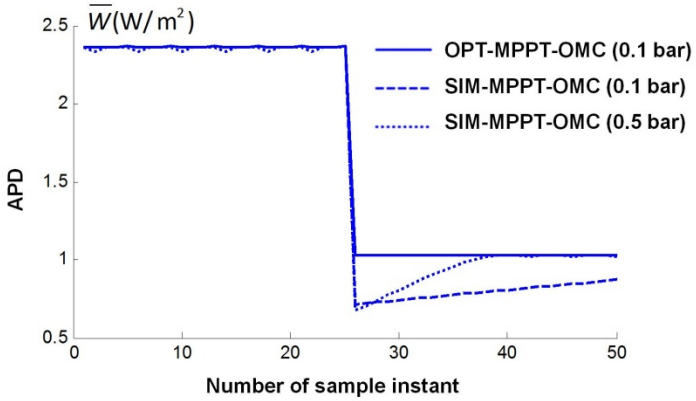

Fig. 14. Osmotic power output with MPPT using P&O algorithm and OMC subject to the variation of the flow rate of the draw.

In addition, the performance of the MPPT with OMC is evaluated by dealing with variation of the draw concentration. The results are shown in Fig. 15 in which the two strategies, OPT-MPPT-OMC and SIM-MPPT-OMC, are studied.

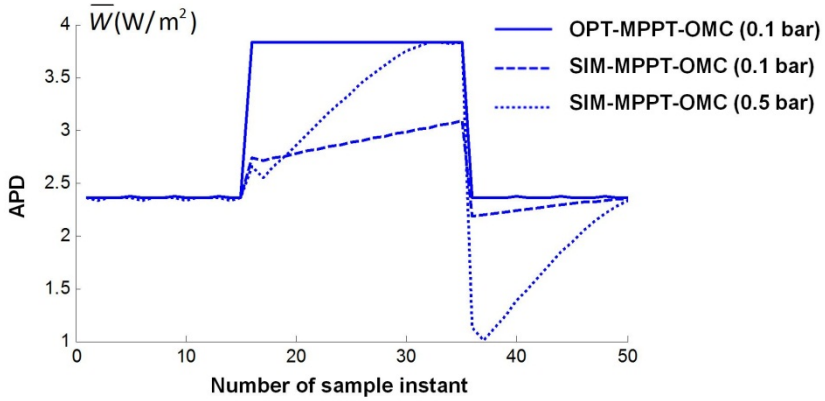

Fig. 15. Osmotic power output with MPPT using P&O algorithm and OMC subject to the variation of the draw concentration.

As shown in Fig 13(b), the concentration of the draw changes two times within the studied period. According to the simulation, the OPT-MPPT-OMC strategy also has good performance to deal with the variations. It is found that fast tracking of the MPP for both the changes of the operations are achieved by OPT-MPPT-OMC. MPP is tracked and stable operation with negligible oscillation of PRO is simulated. In contrast, for the SIM-MPPT-OMC, the larger step-size causes larger fluctuation of the operation due to the changes of the operating condition. Although the SIM-MPPT-OMC with smaller perturbation pressure tracks the MPP slower, it has smaller fluctuation when the operating condition is changed rapidly.

Moreover, a more complex operating condition, co-varied concentration and the flow rate of the draw solution is evaluated. Both the varied profiles of the concentration and flow rate shown in Fig. 13 are studied in a PRO plant with MPPT and OMC. The results are shown in Fig. 16 in which both OPT-MPPT-OMC and SIM-MPPT-OMC strategies are considered. According to the results, the SIM-MPPT-OMC almost fails to track the MPP subject to such complicated varying operating conditions. Both of the SIM-MPPT-OMC with two perturbation pressures cannot respond properly according to the co-varied concentration and flow rate of the draw solution. In contrast, the OPT-MPPT-OMC still performs well that it tracks the MPP fast subject to the rapid and various changes of the salinities. Therefore, based on the knowledge of the PRO process by implementing certain sensors, the performance of the MPPT can be further improved and the OPT-MPPT-OMC is capable to track the varied MPP with the fluctuating salinities.

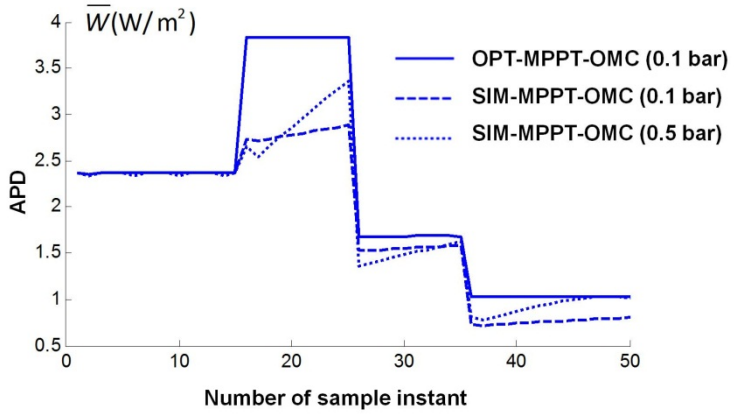

Fig. 16. osmotic power output with MPPT using P&O and OMC subject to co-variant of concentration and flow rate of the salinities.

5. Conclusion

In this study, in order to increase the performance of the scale-up PRO application in practice, MPPT control to achieve the optimum osmotic power output is investigated. First, the process characteristics of the PRO process is studied and evaluated in terms of membrane properties, concentration and flow rate of the salinities. Then, two algorithms for MPPT in PRO are proposed and investigated, including P&O algorithm and IMR algorithm. These MPPT techniques are generic methods to track the MPP, and hence, for further improvement on the MPPT, a model-based OMC is proposed and operated with the MPPT techniques. Finally, a series of simulation are carried out to evaluate the performance of the MPPT and OMC to operate the PRO track the MPP. Based on the results, several conclusions can be drawn: 1) process characteristic of the scale-up PRO process is affected by several factors, such as membrane properties, concentration and flow rate of the salinities etc. Therefore, it is necessary to develop and employ MPPT to ensure the optimum osmotic power output subject to the fluctuating operating conditions. 2) It is demonstrated by simulations that both P&O and IMR algorithms can be used to track the MPP of a PRO process. The trade-off between the rise time and the oscillation by selecting the step-size of the perturbation pressure or incremental pressure exists in both algorithms. Larger step-size results in fast response as well as larger oscillation, and vice versa. 3) Both the MPPT controllers are capable of tracking the varied MPP due to the operating temperature changes. 4) With the availability of several measured variables, OMC is capable to further improve the performance of the MPPT. Based on the model of the scale-up PRO process, an estimated optimum pressure improves the convergence, allows MPPT using a smaller step-size and results in fast response and mitigated oscillation. 5) OMC is capable of quickly adjusting the operation to deal with the rapid changes of the salinities. In the simulation, the OPT-MPPT-OMC performs well to deal with the individual variations of the flow rate or concentration of the draw, and the co-variation of both the influential factors.

Nomenclature

A	Membrane water permeability $[L \cdot m^{-2} \cdot h^{-1} \cdot Pa^{-1}]$
A_m	Membrane area $[m^2]$
B	Membrane solute permeability $[L \cdot m^{-2} \cdot h^{-1}]$

c	Concentration of solution [$kg \cdot kg^{-1}$]
C_{os}	Modified van't Hoff law coefficient [$Pa \cdot kg \cdot g^{-1}$]
D	Diffusion coefficient [$m^2 \cdot s^{-1}$]
E	Specific extractable energy [$kWh \cdot m^{-3}$]
k	Mass transfer coefficient [$m \cdot s^{-1}$]
m	Membrane area allocation rate
J_w	Water permeation flow rate [$L \cdot m^{-2} \cdot h^{-1}$]
J_s	Reverse solute permeation flow rate [$L \cdot m^{-2} \cdot h^{-1}$]
P	Pressure [Pa]
q	Mass flow rate of solution [$kg \cdot h^{-1}$]
S	Membrane structure parameter [m]
V	Volumetric flow rate of solution [$m^3 \cdot h^{-1}$]
W	Membrane power density [$W \cdot m^{-2}$]
$\overline{W}$	Average power density [$W \cdot m^{-2}$]
π	Osmotic pressure [Pa]
ϕ	Dimensionless flow rate
η	Efficiency
ρ	Density of solution [$kg \cdot m^{-3}$]

Abbreviations

APD	Average power density
BP	Boost pump
DPRO	PRO with detrimental effects
ECP	External concentration polarization
ERD	Energy recovery device
HP	High-pressure pump
HT	Hydro-turbine
ICP	Internal concentration polarization
IMR	Incremental mass-resistance
INC	Incremental conductance
IPRO	Ideal PRO process
MPP	Maximum power point
MPPT	Maximum power point tracking
OMC	Optimum model-based controller
P&O	Perturb & observe
PD	Power density
PRO	Pressure retarded osmosis
PV	Photovoltaic
RO	Reverse osmosis
RSP	Reverse solute permeation
SEE	Specific extractable energy
TFC	Thin-film composite

References:

[1] B.E. Logan, M. Elimelech, Membrane-based processes for sustainable power generation using water, Nature, 488 (2012) 313-319.
[2] N.Y. Yip, M. Elimelech, Thermodynamic and Energy Efficiency Analysis of Power Generation from Natural Salinity Gradients by Pressure Retarded Osmosis, Environmental Science & Technology, 46 (2012) 5230-5239.
[3] N.Y. Yip, M. Elimelech, Influence of Natural Organic Matter Fouling and Osmotic Backwash on Pressure Retarded Osmosis Energy Production from Natural Salinity Gradients, Environmental Science & Technology, 47 (2013) 12607-12616.
[4] H. Wei, W. Yang, M.H. Shaheed, Modelling and simulation of osmotic energy from salinity gradients: A case study from River Thames, in: Renewable Energy Research and Applications (ICRERA), 2013 International Conference on, 2013, pp. 907-912.
[5] W. He, Y. Wang, A. Sharif, M.H. Shaheed, Thermodynamic analysis of a stand-alone reverse osmosis desalination system powered by pressure retarded osmosis, Desalination, 352 (2014) 27-37.
[6] W. He, Y. Wang, M.H. Shaheed, Energy and thermodynamic analysis of power generation using a natural salinity gradient based pressure retarded osmosis process, Desalination, 350 (2014) 86-94.
[7] S.E. Skilhagen, J.E. Dugstad, R.J. Aaberg, Osmotic power — power production based on the osmotic pressure difference between waters with varying salt gradients, Desalination, 220 (2008) 476-482.
[8] S.E. Skilhagen, Osmotic power — a new, renewable energy source, Desalination and Water Treatment, 15 (2010) 271-278.
[9] N.Y. Yip, M. Elimelech, Performance Limiting Effects in Power Generation from Salinity Gradients by Pressure Retarded Osmosis, Environmental Science & Technology, 45 (2011) 10273-10282.
[10] X. Li, T.-S. Chung, Thin-film composite P84 co-polyimide hollow fiber membranes for osmotic power generation, Applied Energy, 114 (2014) 600-610.
[11] F. Helfer, C. Lemckert, Y.G. Anissimov, Osmotic power with Pressure Retarded Osmosis: Theory, performance and trends – A review, Journal of Membrane Science, 453 (2014) 337-358.
[12] Y.C. Kim, Y. Kim, D. Oh, K.H. Lee, Experimental Investigation of a Spiral-Wound Pressure-Retarded Osmosis Membrane Module for Osmotic Power Generation, Environmental Science & Technology, 47 (2013) 2966-2973.
[13] A.P. Straub, S. Lin, M. Elimelech, Module-Scale Analysis of Pressure Retarded Osmosis: Performance Limitations and Implications for Full-Scale Operation, Environmental Science & Technology, (2014).
[14] S. Lin, A.P. Straub, M. Elimelech, Thermodynamic limits of extractable energy by pressure retarded osmosis, Energy & Environmental Science, 7 (2014) 2706-2714.
[15] L.D. Banchik, M.H. Sharqawy, J.H. Lienhard V, Limits of power production due to finite membrane area in pressure retarded osmosis, Journal of Membrane Science, 468 (2014) 81-89.
[16] B.J. Feinberg, G.Z. Ramon, E.M.V. Hoek, Scale-up characteristics of membrane-based salinity-gradient power production, Journal of Membrane Science, 476 (2015) 311-320.
[17] E. Sivertsen, T. Holt, W.R. Thelin, G. Brekke, Iso-watt diagrams for evaluation of membrane performance in pressure retarded osmosis, Journal of Membrane Science, 489 (2015) 299-307.
[18] A. Altaee, A. Sharif, G. Zaragoza, Limitations of osmotic gradient resource and hydraulic pressure on the efficiency of dual stage PRO process, Renewable Energy, 83 (2015) 1234-1244.
[19] A. Altaee, A. Sharif, G. Zaragoza, N. Hilal, Dual stage PRO process for power generation from different feed resources, Desalination, 352 (2014) 118-127.
[20] A. Altaee, N. Hilal, Design optimization of high performance dual stage pressure retarded osmosis, Desalination, 355 (2015) 217-224.
[21] A. Altaee, N. Hilal, Dual stage PRO power generation from brackish water brine and wastewater effluent feeds, Desalination.
[22] A. Altaee, N. Hilal, Dual-stage forward osmosis/pressure retarded osmosis process for hypersaline solutions and fracking wastewater treatment, Desalination, 350 (2014) 79-85.

[23] A. Altaee, A. Sharif, G. Zaragoza, A.F. Ismail, Evaluation of FO-RO and PRO-RO designs for power generation and seawater desalination using impaired water feeds, Desalination, 368 (2015) 27-35.
[24] G. Han, J. Zuo, C. Wan, T.-S. Chung, Hybrid pressure retarded osmosis-membrane distillation (PRO-MD) process for osmotic power and clean water generation, Environmental Science: Water Research & Technology, 1 (2015) 507-515.
[25] J.-G. Lee, Y.-D. Kim, S.-M. Shim, B.-G. Im, W.-S. Kim, Numerical study of a hybrid multi-stage vacuum membrane distillation and pressure-retarded osmosis system, Desalination, 363 (2015) 82-91.
[26] W. He, Y. Wang, M.H. Shaheed, Stand-alone seawater RO (reverse osmosis) desalination powered by PV (photovoltaic) and PRO (pressure retarded osmosis), Energy, 86 (2015) 423-435.
[27] B.C. McCool, A. Rahardianto, J. Faria, K. Kovac, D. Lara, Y. Cohen, Feasibility of reverse osmosis desalination of brackish agricultural drainage water in the San Joaquin Valley, Desalination, 261 (2010) 240-250.
[28] D.D. Anastasio, J.T. Arena, E.A. Cole, J.R. McCutcheon, Impact of temperature on power density in closed-loop pressure retarded osmosis for grid storage, Journal of Membrane Science, 479 (2015) 240-245.
[29] K. Touati, C. Hänel, F. Tadeo, T. Schiestel, Effect of the feed and draw solution temperatures on PRO performance: Theoretical and experimental study, Desalination, 365 (2015) 182-195.
[30] K. Touati, F. Tadeo, C. Hänel, T. Schiestel, Effect of the operating temperature on hydrodynamics and membrane parameters in pressure retarded osmosis, Desalination and Water Treatment, (2015) 1-13.
[31] A. Achilli, J.L. Prante, N.T. Hancock, E.B. Maxwell, A. Childress, Experimental Results from RO-PRO: A Next Generation System for Low-Energy Desalination, Environmental Science & Technology, (2014).
[32] Q. She, X. Jin, C.Y. Tang, Osmotic power production from salinity gradient resource by pressure retarded osmosis: Effects of operating conditions and reverse solute diffusion, Journal of Membrane Science, 401–402 (2012) 262-273.
[33] W. He, Y. Wang, M.H. Shaheed, Enhanced energy generation and membrane performance by two-stage pressure retarded osmosis (PRO), Desalination, 359 (2015) 186-199.
[34] K. Yeong-Chan, L. Tsorng-Juu, C. Jiann-Fuh, Novel maximum-power-point-tracking controller for photovoltaic energy conversion system, Industrial Electronics, IEEE Transactions on, 48 (2001) 594-601.
[35] S. Jain, V. Agarwal, A new algorithm for rapid tracking of approximate maximum power point in photovoltaic systems, Power Electronics Letters, IEEE, 2 (2004) 16-19.
[36] N. Femia, G. Petrone, G. Spagnuolo, M. Vitelli, Optimization of perturb and observe maximum power point tracking method, Power Electronics, IEEE Transactions on, 20 (2005) 963-973.
[37] A. Pandey, N. Dasgupta, A.K. Mukerjee, Design Issues in Implementing MPPT for Improved Tracking and Dynamic Performance, in: IEEE Industrial Electronics, IECON 2006 - 32nd Annual Conference on, 2006, pp. 4387-4391.
[38] G. Kumar, M.B. Trivedi, A.K. Panchal, Innovative and precise MPP estimation using P–V curve geometry for photovoltaics, Applied Energy, 138 (2015) 640-647.
[39] J. Ahmed, Z. Salam, A Maximum Power Point Tracking (MPPT) for PV system using Cuckoo Search with partial shading capability, Applied Energy, 119 (2014) 118-130.
[40] S.A. Rizzo, G. Scelba, ANN based MPPT method for rapidly variable shading conditions, Applied Energy, 145 (2015) 124-132.
[41] N. Bizon, On tracking robustness in adaptive extremum seeking control of the fuel cell power plants, Applied Energy, 87 (2010) 3115-3130.
[42] N. Bizon, Energy harvesting from the FC stack that operates using the MPP tracking based on modified extremum seeking control, Applied Energy, 104 (2013) 326-336.
[43] Z. Salam, J. Ahmed, B.S. Merugu, The application of soft computing methods for MPPT of PV system: A technological and status review, Applied Energy, 107 (2013) 135-148.

[44] J. Ahmed, Z. Salam, An improved perturb and observe (P&O) maximum power point tracking (MPPT) algorithm for higher efficiency, Applied Energy, 150 (2015) 97-108.
[45] C.-H. Lin, C.-H. Huang, Y.-C. Du, J.-L. Chen, Maximum photovoltaic power tracking for the PV array using the fractional-order incremental conductance method, Applied Energy, 88 (2011) 4840-4847.
[46] K. Gerstandt, K.V. Peinemann, S.E. Skilhagen, T. Thorsen, T. Holt, Membrane processes in energy supply for an osmotic power plant, Desalination, 224 (2008) 64-70.
[47] W. He, Y. Wang, M.H. Shaheed, Modelling of osmotic energy from natural salt gradients due to pressure retarded osmosis: Effects of detrimental factors and flow schemes, Journal of Membrane Science, 471 (2014) 247-257.
[48] B.D. Freeman, Basis of Permeability/Selectivity Tradeoff Relations in Polymeric Gas Separation Membranes, Macromolecules, 32 (1999) 375-380.
[49] A. Mehta, A.L. Zydney, Permeability and selectivity analysis for ultrafiltration membranes, Journal of Membrane Science, 249 (2005) 245-249.
[50] L.M. Robeson, Correlation of separation factor versus permeability for polymeric membranes, Journal of Membrane Science, 62 (1991) 165-185.
[51] J.L. Prante, J.A. Ruskowitz, A.E. Childress, A. Achilli, RO-PRO desalination: An integrated low-energy approach to seawater desalination, Applied Energy, 120 (2014) 104-114.
[52] M.H. Sharqawy, L.D. Banchik, J.H. Lienhard V, Effectiveness–mass transfer units (ε–MTU) model of an ideal pressure retarded osmosis membrane mass exchanger, Journal of Membrane Science, 445 (2013) 211-219.
[53] L.D. Banchik, M.H. Sharqawy, J.H. Lienhard V, Effectiveness-mass transfer units (ε-MTU) model of a reverse osmosis membrane mass exchanger, Journal of Membrane Science, 458 (2014) 189-198.
[54] G.A. Fimbres-Weihs, D.E. Wiley, Numerical study of two-dimensional multi-layer spacer designs for minimum drag and maximum mass transfer, Journal of Membrane Science, 325 (2008) 809-822.
[55] S.C. Chen, C.F. Wan, T.-S. Chung, Enhanced fouling by inorganic and organic foulants on pressure retarded osmosis (PRO) hollow fiber membranes under high pressures, Journal of Membrane Science, 479 (2015) 190-203.
[56] Y.C. Kim, J.H. Lee, S.-J. Park, Novel crossflow membrane cell with asymmetric channels: Design and pressure-retarded osmosis performance test, Journal of Membrane Science, 476 (2015) 76-86.
[57] G. Han, Q. Ge, T.-S. Chung, Conceptual demonstration of novel closed-loop pressure retarded osmosis process for sustainable osmotic energy generation, Applied Energy, 132 (2014) 383-393.
[58] X. Song, Z. Liu, D.D. Sun, Energy recovery from concentrated seawater brine by thin-film nanofiber composite pressure retarded osmosis membranes with high power density, Energy & Environmental Science, 6 (2013) 1199-1210.
[59] S. Chou, R. Wang, L. Shi, Q. She, C. Tang, A.G. Fane, Thin-film composite hollow fiber membranes for pressure retarded osmosis (PRO) process with high power density, Journal of Membrane Science, 389 (2012) 25-33.
[60] A. Achilli, T.Y. Cath, A.E. Childress, Power generation with pressure retarded osmosis: An experimental and theoretical investigation, Journal of Membrane Science, 343 (2009) 42-52.
[61] A.R. Bartman, A. Zhu, P.D. Christofides, Y. Cohen, Minimizing energy consumption in reverse osmosis membrane desalination using optimization-based control, Journal of Process Control, 20 (2010) 1261-1269.
[62] A.R. Bartman, P.D. Christofides, Y. Cohen, Nonlinear model-based control of an experimental reverse-osmosis water desalination system, Industrial & Engineering Chemistry Research, 48 (2009) 6126-6136.
[63] K.M. Sassi, I.M. Mujtaba, Optimal operation of RO system with daily variation of freshwater demand and seawater temperature, Computers & Chemical Engineering, 59 (2013) 101-110.